ELSEVIER

Journal of Power Sources 103 (2002) 230–236

JOURNAL OF POWER SOURCES

www.elsevier.com/locate/jpowsour

Corrosion resistance of the intermetallic compound, NiAl, in a molten carbonate fuel cell environment

Xu Songbo[a,*], Zhu Yongda[b], Huang Xing[b], Zhou Bangna[b], Yu Zhongxing[b]

[a]*Department of Chemical Engineering, University of New Brunswick, New Brunswick, Box 4400, Canada E3B 5A3*
[b]*Department of Material Science and Engineering, Shanghai University, Shanghai, PR China*

Received 26 June 2001; accepted 5 July 2001

Abstract

The corrosion resistance of intermetallic NiAl, superalloy GH217 and an 18-8 stainless steel in molten carbonates at 923 K was determined by weight loss and electrochemical measurements. Morphology and structure of the corrosion products were characterized using a combination of electron probe and X-ray diffraction (XRD). The corrosion resistance of NiAl is the best among the materials investigated. NiAl produces more protective corrosion products and forms more complete oxide films on the surface than GH217 or 18-8 stainless steel.

Keywords: Corrosion resistance; Molten carbonate; Intermetallic compound NiAl

1. Introduction

Molten carbonate fuel cells (MCFCs) are energy conversion devices that directly convert chemical energy in fossil fuels into electricity. MCFCs are operated in molten carbonate at about 923 K. The life of cells is limited by the corrosion of structural materials such as wet-seal materials in cells [1]. MgO ceramics and several precious metals have good corrosion resistance in molten carbonate, but the very poor mechanical properties of MgO ceramics and the cost of precious metals prevent them from being applied in MCFCs [2,3]. Now, stainless steels are used in MCFCs, but their corrosion resistance in molten carbonate does not satisfy the need of a 40,000 h lifetime, especially, in the wet seal area under highly corrosive carbonate melt [1]. Recently, the corrosion behavior of Fe, Ni and Cr, the most important elements in stainless steels and superalloys, has been studied [4–6]. Vossen [4] reported that, the NiO passive film on nickel in molten Li_2CO_3–K_2CO_3 decrease the potectivity of passive film due to Ni^{3+} formation at more positive potential. Iron in Ni–Fe alloys can form Fe^{3+} ion in NiO film, and ferric ion make corrosion current increase [5]. The passive film of Cr in molten carbonate can solve at more positive potential. Chromium is not suitable to improve the corrosion resistance in molten carbonate [6].

Hwang and Kang [7] suggested that aluminum-containing alloys possess sufficient corrosion resistance under wet-seal area environment in MCFCs and aluminizing can be selected as the technique for protection. Hwang and coworkers [7–9] reported Al–Ni-plated materials have excellent corrosion resistance in carbonate melts and NiAl among the intermetallic phases of $NiAl_3$, Ni_2Al_3, NiAl in the Al–Ni coated layers plays important roles. But, the development of voids between the coated layer and the substrate make the coated layer failure after a long-term immersion.

NiAl is a material of great interest in high temperature applications because of its high melting point and excellent oxidation resistance. As yet NiAl is used mainly as a base material for oxidation resistant coatings on high-temperature alloys. Renewed interest has arisen because of improvements in mechanical properties and its good ductility at high temperature [10]. It is intended to use NiAl in structural applications. NiAl oxidation behavior has been investigated in recent years [11,12], but there are a few corrosion data for NiAl in molten carbonate.

In this paper, the corrosion behavior of intermetallic NiAl was studied in molten carbonate, and was compared with those of an 18-8 stainless steel and superalloy GH217 by immersion and electrochemical tests. The effects of aluminum, nickel, chromium, iron and corrosion products on corrosion are discussed.

* Corresponding author. Tel.: +506-454-4491; fax: +506-453-3591.
E-mail address: sbxu@unb.ca (X. Songbo).

0378-7753/02/$ – see front matter
PII: S0378-7753(01)00854-0

Table 1
Compositions in wt.% of the materials investigated

Elements	C	Ni	Al	Cr	Fe	Ti	Co	Mo	Mn	Si	W	P	S
NiAl	–	70.69	Bal.	–	–	–	–	–	–	–	–	–	–
Superalloy GH217	0.1	Bal.	0.72	23.26	–	2.18	10.05	1.2	–	–	1.64	–	–
18-8 Stainless steel	0.06	9.7	–	18.12	Bal.	0.56	–	–	1.05	0.39	–	0.032	0.009

2. Experimental

NiAl was prepared by induction melting and casting into an ingot. The 18-8 stainless steel and superalloy GH217 were commercial materials. The compositions of three materials are given in Table 1. The materials were cut into specimens (1 mm × 10 mm × 15 mm and 1 mm × 1 mm × 50 mm) which were used in immersion tests and electrochemical tests, respectively, by spark erosion and abraded to 1000 grit on all sides. It was ascertained that further polishing had no influence on the corrosion processes.

Immersion experiments were performed in an alumina pot, which contained molten carbonate in a furnace kept at 923 ± 2 K. The carbonate is a mixture of 62 mol% Li_2CO_3 and 38 mol% K_2CO_3. The specimens (1 mm × 10 mm × 15 mm) were rinsed with acetone to remove grease. The specimens were measured the weights and sizes before immersion in molten salt. The immersion of materials investigated in molten carbonate, respectively, lasted for 4, 8, 12, 24, 36, 54, 72, 100, 120 h. After immersion, the specimens were rinsed with distilled water, dipped in a solution containing hydrochloric acid and tetrabutylammonium iodide to strip corrosion products, dried, and weighted by microbalance. The morphology and distribution of elements of oxide scales on the surface of specimens were investigated with electron probe. The structures of corrosion products were studied with X-ray diffraction (XRD).

Electrochemical tests were carried out in an alumina crucible containing carbonate melt. A silver ring counter electrode was placed near the inner wall of the cell, and working and reference electrodes were placed near the center. The reference electrode consisted of an alumina tube filled with molten salts (60 mol% KCl + 40 mol% LiCl + 0.1 mol% AgCl) in which a silver wire was inserted. The working electrode (1 mm × 1 mm × 50 mm) was connected with a copper wire which was sealed in an alumina tube with Al_2O_3 powder and a binder. The working electrode protruding from the tube polished to 1000 grit, washed with distilled water and acetone, and then dried before tests. The electrochemical set-up consisted of a ZF-3 potentiostat, an X–Y recorder and a signal generator.

3. Results and discussion

The time-dependent weight loss of NiAl, 18-8 stainless steel and GH217 superalloy in molten carbonate at 923 K is shown in Fig. 1. The weight loss of NiAl is much less than those of superalloy GH217 and 18-8 stainless steel, especially, after 50 h, and superalloy GH217 and 18-8 stainless steel show the corrosion rate increase suddenly after ~50 h.

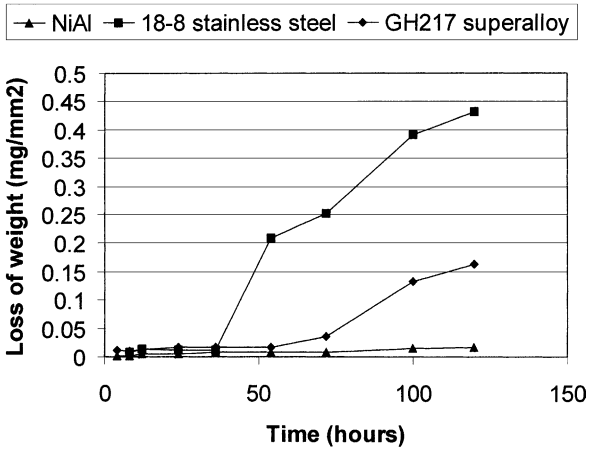

Fig. 1. The weight loss of NiAl, GH217 superalloy and 18-8 stainless steel in carbonate melt (923 K).

The electron probe micrographs of NiAl after immersion in molten carbonate for 24 h at 923 K are shown in Fig. 2a. A continuous oxide film can be observed on NiAl. The element distribution on NiAl is shown in Fig. 2b and c. Nickel and aluminum distributed evenly on surface of NiAl. The morphology of film on superalloy GH217 after immersion in molten carbonate is shown in Fig. 3(a). The oxide film on GH217 is composed of two regions. One is bright, rich in Cr, the other is dark, rich in Ni.

An electron probe micrographs of 18-8 stainless steel after immersion in carbonate are shown in Fig. 4a. The film on stainless steel is composed of particles of corrosion products. The element distributions (Fig. 4b–d) show that the particles contain more iron and less chromium and nickel than the base alloy.

The XRD results are shown in Table 2. The corrosion products on NiAl after immersion for 120 h are composed of $LiAlO_2$ and $Li_2Ni_8O_{10}$. Those on GH217 and 18-8 stainless

Table 2
The corrosion products on the samples investigated after immersion in carbonate for 120 h

Samples	Corrosion products
NiAl	$LiAlO_2 + Li_2Ni_8O_{10}$
GH217 superalloy	$Ni_2O_3 + Li_2Ni_8O_{10} + LiCrO_2$
18-8 Stainless steel	$LiFeO_2 + Li_2Ni_8O_{10} + LiCrO_2$

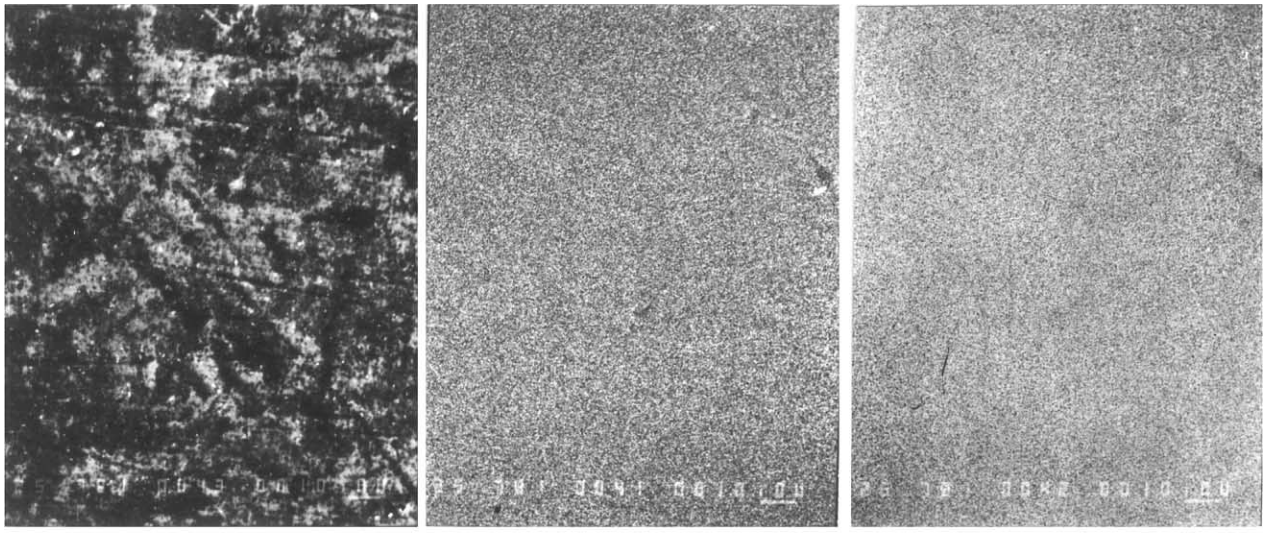

(a) (b) (c)

Fig. 2. Oxide film morphology and element distribution for NiAl immersed in molten carbonate at 923 K for 24 h: (a) morphology; (b) aluminum distribution and (c) nickel distribution.

steel are, respectively, $Ni_2O_3 + Li_2Ni_8O_{10} + LiCrO_2$ and $LiFeO_2 + Li_2Ni_8O_{10} + LiCrO_2$.

Fig. 5 shows the cyclic voltammograms for three materials immersed in molten carbonate at 923 K. All voltammograms show the active, passive and transpassive regions. Pitting potentials, repassivation potentials and free corrosion potentials are shown in Table 3. Fig. 6 shows the anodic curves with different sweep rates. As can be seen, potentials corresponding peak currents vary with sweep rates.

The free corrosion of NiAl in molten carbonate is mainly attributed to electrochemical reaction processes. Possible cathodic reactions have been described as oxygen reductions as follows:

$$O_2 + 2CO_3^{2-} = 2O_2^{2-} + 2CO_2 \quad (1)$$

$$O_2 + O_2^{2-} = 2O_2^{-} \quad (2)$$

Table 3
Pitting potential, repassivation potential and free corrosion potential of three alloys

Alloys	Pitting potential (mV)	Repassivation potential (mV)	Free corrosion potential (mV)
NiAl	400	−300	−800
18-8 Stainless steel	350	−350	−800
GH217 superalloy	340	−450	−400

$$O_2^{-} + e = O_2^{2-} \quad (3)$$

$$O_2^{2-} + e = O^{2-} + O^{-} \quad (4)$$

$$O^{-} + e = O^{2-} \quad (5)$$

$$O^{2-} + CO_2 = CO_3^{2-} \quad (6)$$

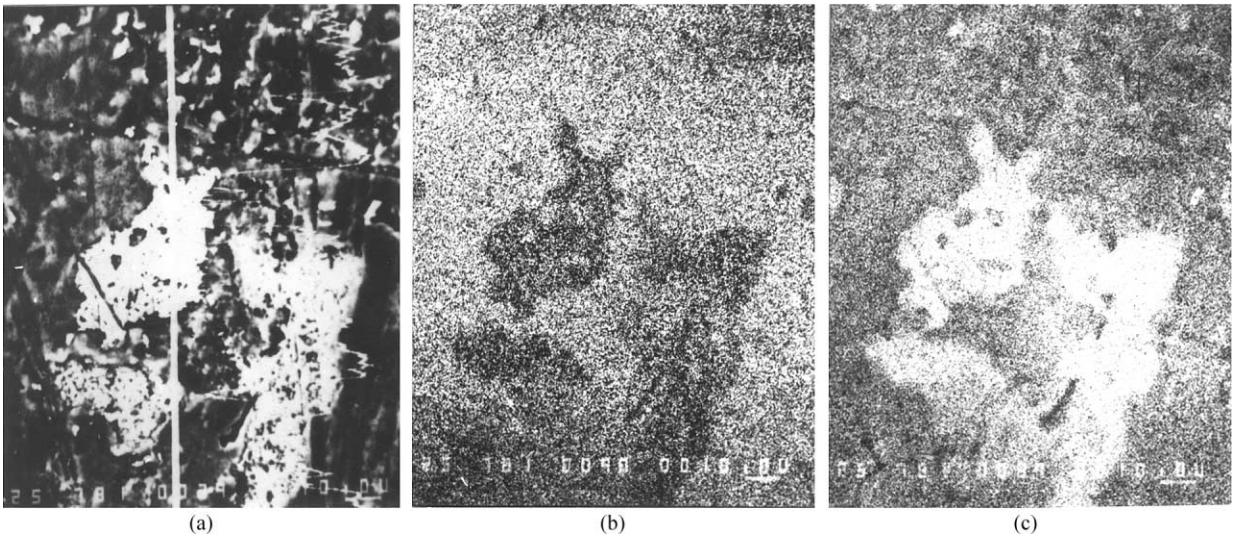

(a) (b) (c)

Fig. 3. Oxide film morphology and element distribution for superalloy GH217 immersed in molten carbonate at 923 K for 24 h: (a) morphology; (b) Ni distribution and (c) Cr distribution.

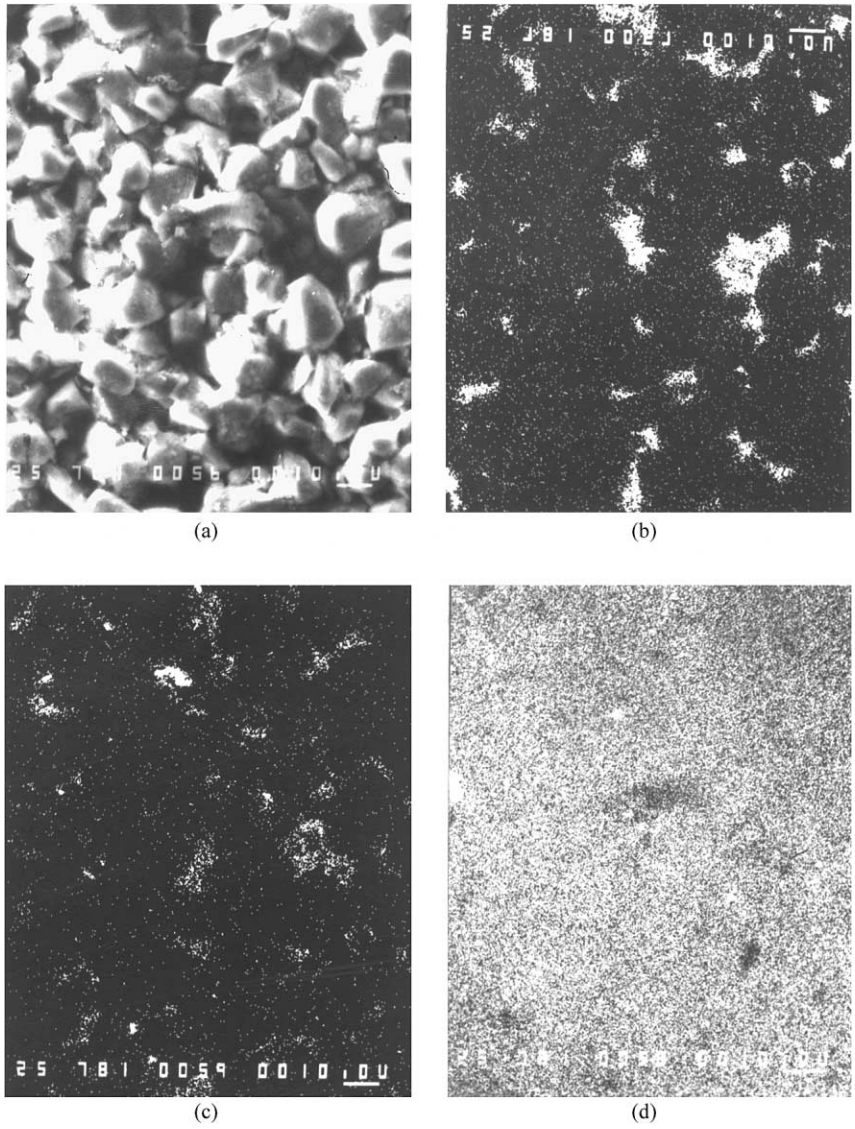

Fig. 4. Oxide film morphology and element distribution for 18-8 stainless steel immersed in molten carbonate at 923 K for 24 h: (a) morphology; (b) Cr distribution; (c) Ni distribution and (d) Fe distribution.

The reactions to limit, the oxygen reduction rate are reactions (3) and (4), i.e. the reduction of peroxide ions and superoxide ions [13–16].

The anodic reactions in molten carbonate can be represented by Eqs. (7)–(10) [6,17–19].

$$M = M^{2+} + 2e \quad (7)$$

$$M + O^{2-} = MO + 2e \quad (8)$$

$$M + 2OH^{-} = MO + H_2O + 2e \quad (9)$$

$$M + {CO_3}^{2-} = MO + CO_2 + 2e \quad (10)$$

The metals may dissolve directly in electrolyte on the basis of Eq. (7). The change of the electrolytes color after immersion of samples for a period of time verified that metallic ions occurred in the electrolyte, that was to say, dissolution reactions existed. The metals may also react directly with oxidizing ions and produce oxides on the surface of alloys according to Eqs. (8)–(10). The appearance of coherent oxides on alloys was likely to results from these reactions.

During immersion in molten carbonate, initially, NiAl dissolved actively, as shown in the active stage in Fig. 5. This was an irreversible processes due to the variation of peak currents with scan rates (Fig. 6). Aluminum in NiAl may preferentially dissolve or react with oxidizing ions, because of its higher activity. With the development of the anodic reactions, the oxide films formed on the surface of NiAl and inhibited the further oxidization of the base alloy. It shows a passive stage in Fig. 5. The element distributions of Ni and Al show that the compositions of the oxide films on NiAl are uniform (Fig. 2b and c). XRD shows that the oxide layers on NiAl were composed of and $Li_2Ni_8O_{10}$ and $LiAlO_2$. The results from Auger spectrum in passive films on NiAl in

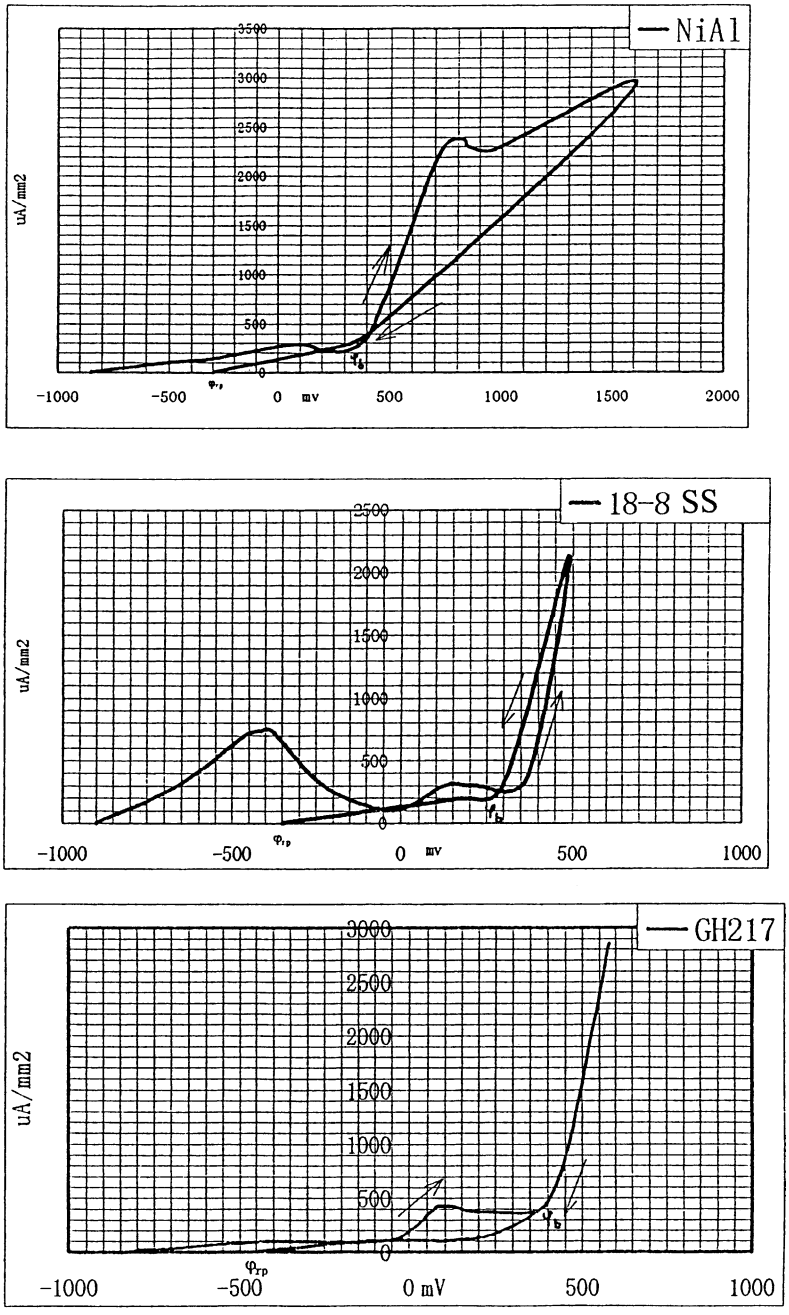

Fig. 5. The cyclic voltammograms of NiAl, GH217 and 18-8 stainless steel in molten carbonate at 923 K.

molten carbonate also show that the outer-layer is rich in Al and the inner-layer is rich in Ni [20]. Thus, it is reasonable to believe that the outer-layer oxide on NiAl was rich in $LiAlO_2$ and the inner-layer was rich in $Li_2Ni_8O_{10}$. $LiAlO_2$ was the product of aluminum oxide by lithiation process. The lithiation reactions also occurred in inner-layer nickel oxide by diffusion of Li and O, ($Li_2O + NiO + (1/2)O_2 = 2LiNiO_2$) [21]. Due to less oxygen in melts under air atmosphere and the difficult of diffusion through outer-layer $LiAlO_2$, the incomplete lithiation process of NiO led to the products of $Li_2Ni_8O_{10}$ ($Li_2Ni_8O_{10}$ can be regarded as $2LiNiO_2 + 6NiO$). The outer-layer $LiAlO_2$ is very resistant to corrosion in carbonate melts [7–9,22–24]. Thus, $LiAlO_2$ is responsible for the least weight loss of NiAl in the three alloys. From the cyclic potentiodynamic curves (Fig. 5), the pitting potential and the repassivation potential of NiAl are the most positive among three alloys. These also indicated the oxide films on NiAl are the best in corrosion resistance in molten carbonate.

Unlike NiAl, the 18-8 stainless steel formed an oxide film composed of particle corrosion products (Fig. 4a). The element distribution of oxide film (Fig. 4b–d) and the results of XRD indicated that these particles were mainly iron oxides $LiFeO_2$. Zhu et al. [25] studied the corrosion of

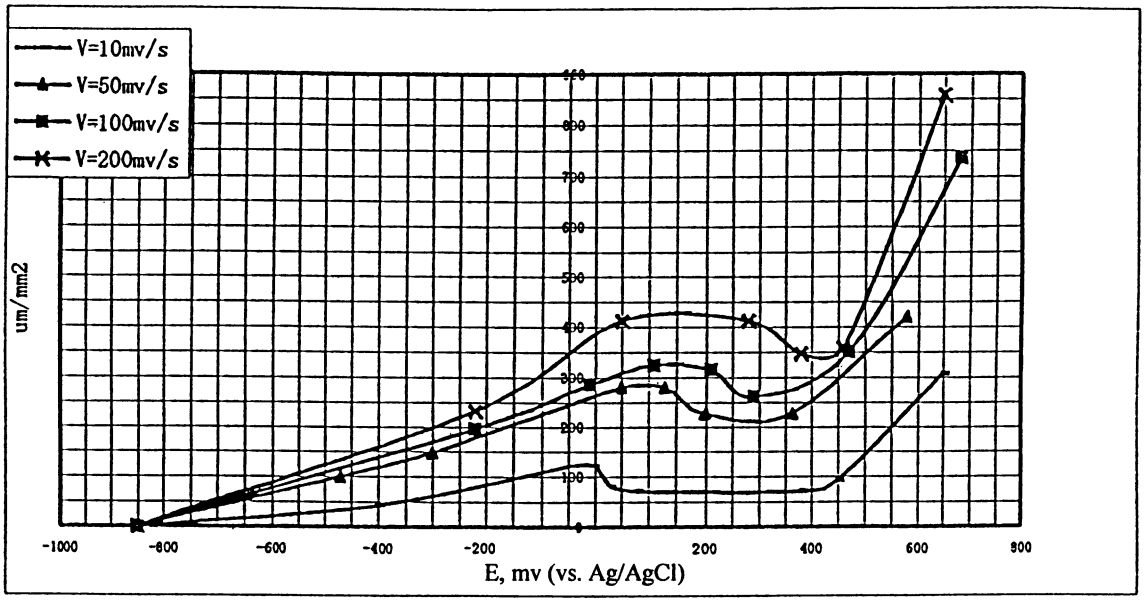

Fig. 6. The potentiodynamic curves of NiAl at different scan rates.

SS310 and SS316 in molten carbonate and reported that the corrosion products on stainless steel consist of two layers. The outer-layer was porous, the inner-layer was quite compact and may have some small pores. The oxide films on 18-8 stainless steel may be made up of outer-layer rich in $LiFeO_2$ particles and inner-layer composed mainly of $Li_2Ni_8O_{10}$, and $LiCrO_2$ (Table 2). Generally, $LiCrO_2$ can protect the base alloy from further corrosion. The higher the concentration of chromium in alloys, the lower the corrosion rate [25]. However, in carbonate melts, $LiCrO_2$ may react as follow [26,27]:

$$2LiCrO_2 + 3CO_3^{2-} = 2CrO_4^{2-} + Li_2CO_3 + 3CO_2 + 6e$$

$$2LiCrO_2 + 4CO_2 + 6e = 2Cr + Li_2CO_3 + 3CO_3^{2-}$$

Cr^{3+} in $LiCrO_2$ is not very stable. It can be oxidized to Cr^{6+} in CrO_4^{2-} or reduced to Cr. The more negative pitting potential of 18-8 stainless steel compared with NiAl in Fig. 5 indicated the poorer protectivity of $LiCrO_2$ than $LiAlO_2$. Thus, the weight loss of 18-8 stainless steel is more than NiAl. The oxide films on the superalloy GH217 consist of nickel-rich phases (mainly Ni_2O_3 and $Li_2Ni_8O_{10}$) and chromium-rich phases (mainly $LiCrO_2$) in Fig. 3. Xie et al. [28,29] demonstrated that Ni^{3+} was likely to decomposed according to $Ni_2O_3 = 2NiO + (1/2)O_2$, and $LiCrO_2$ is not very protective in the carbonate melts as discussed above. The weight loss of GH217 is more in molten carbonate.

4. Conclusions

1. The weight loss of alloys investigated shows that the corrosion resistance of NiAl in molten carbonate at 923 K is better than that of 18-8 stainless steel or superalloy GH217.
2. The oxide film on NiAl in molten carbonate are uniform, and the oxide layer on superalloy GH217 are composed of two regions, respectively, rich in Ni and Cr. The oxide layer on 18-8 stainless steel are made up of outer particles rich in Fe and the inner oxides of Cr and Ni.
3. The corrosion products of NiAl after immersion for 120 h are composed of $LiAlO_2$ and $Li_2Ni_8O_{10}$. The corrosion products of GH217 and 18-8 stainless steel, respectively, consist of $Ni_2O_3 + Li_2Ni_8O_{10} + LiCrO_2$ and $LiFeO_2 + Li_2Ni_8O_{10} + LiCrO_2$.
4. Superalloy GH217 and 18-8 stainless steel show, respectively, sudden increase of corrosion after immersion in molten carbonate for 36 and 54 h.
5. The pitting potential of NiAl is the most positive among three alloys and its potentials of peak current change with the sweep rates.

References

[1] A.J. Appleby, F.R. Foulkes, Fuel Cell Handbook, Van Nostrand Reinhold, New York, 1989.
[2] G.J. Janz, A. Conte, Electrochim. Acta 9 (1964) 1269–1279.
[3] M.D. Ingram, G.J. Janz, Electrochim. Acta 10 (1965) 783.
[4] J.P.T. Vossen, in: Proceeding of The Third International Symposium on Cell Technology, Vol. Pv93-3, p. 278.
[5] J.P.T. Vossen, A.H.H. Janssen, J.H.W. de Wit, J. Electrochem. Soc. 143 (1996) 58–65.
[6] J.P.T. Vossen, R.C. Makkus, J. Electrochem Soc. 143 (1996) 66.
[7] E.R. Hwang, S.G. Kang, J. Power Sources 76 (1998) 48–53.
[8] N. Fujimoto, M. Yamamoto, T. Nagoya, J. Power Sources 71 (1998) 231–238.
[9] Y. Kawabata, N. Fujimoto, M. Yamamoto, T. Nagoya, M. Nishida, J. Power Sources 86 (2000) 324–328.
[10] G. Sauthoff, Z. Metallkde 81 (1990) 855.

[11] G.C. Rybicki, J.L. Smialek, Oxid. Metals 32 (1989) 431.
[12] M.W. Brumm, H.J. Grabke, Corros. Sci. 33 (1992) 1677–1690.
[13] M.W. Brumm, H.J. Grabke, B. Wagemann, Corros. Sci. 36 (1994) 37–53.
[14] I. Uchida, T. Nishina, Y. Mugikura, K. Itaya, J. Electroanal. Chem. 206 (1986) 229.
[15] C. Yuh, J.R. Selman, AIChE J. 34 (1988) 1949.
[16] T. Nishina, I. Uchida, in: Proceedings of the Symposium on Molten Carbonate Fuel Cell Technology, Vol. Pv90-16, The Electrochemical Society, 1990, p. 438.
[17] T. Nishina, G. Lindbergh, T. Kudo, I. Uchida, in: Proceedings of the International Fuel Cell Conference, NEDO, 1992, pp. 189–192.
[18] R.A. Donado, L.G. Marianowski, H.C. Maru, J.R. Selman, J. Electrochem. Soc. 131 (1984) 2535.
[19] H.S. Hsu, J.H. Devan, J. Electrochem. Soc. 133 (1986) 2077.
[20] J.P.T. Vossen, L. Plomp, J.H.W. de Wit, J. Electrochem. Soc. 141 (1994) 3040.
[21] H. Xing, X. Songbo, Z. Bangna, J. Shanghai Univ. 6 (2000) 199–202.
[22] P. Tomczyk, G. Mordarski, J. Oblakowski, J. Electroanal. Chem. 353 (1993) 177.
[23] P.A. Shores, M.J. Pischke, The hot corrosion of current collector, separators in carbonate fuel cells, in: Proceedings of The Third Symposium on Molten Carbonate Fuel Cell Technology, Vol. Pv93-3, Electrochemical Society, p. 214.
[24] C.Y. Yuh, P. Singh, L. Paetsch, H.C. Maru, Corros. 87 (1987) 176.
[25] B. Zhu, G. Lindbergh, D. Simonsson, Corros. Sci. 41 (1999) 1515–1528.
[26] B. Zhu, G. Lindbergh, D. Simonsson, Corros. Sci. 41 (1999) 1497–1513.
[27] P. Biedenkopf, M. Spiegel, H.J. Grabke, Electrochim. Acta 44 (1998) 683–692.
[28] G. Xie, Y. Sakamura, K. Ema, Y. Ito, J. Power Sources 32 (1990) 125.
[29] G. Xie, Y. Sakamura, K. Ema, Y. Ito, J. Power Sources 32 (1990) 135.